Interlayer growth kinetics of a binary solid-solution based on the thermodynamic extremal principle: Application to the formation of spinel at periclase-corundum contacts: ELECTRONIC SUPPLEMENTARY MATERIAL

March 8, 2016

1 Explicit expressions as used in numerical scheme for calculating system evolution

1.1 Partial derivatives of dotg (Eq. 14) with respect to the six kinetic variables

```
The six kinetic variables are: rLdot, rRdot, ua, vc, uc, vb  ddot grLdot = -((1/(12*omegac))*((6*wone+9*rL^2*wthree+6*rL*rR*wthree+3*rR^2*wthree+8*rL*wtwoe+4*rR*wtwoe)*(xL-xR))) \\ ddot grRdot = -((1/(12*omegac))*((6*wone+3*rL^2*wthree+6*rL*rR*wthree+9*rR^2*wthree+4*rL*wtwoe+8*rR*wtwoe)*(xL-xR))) \\ ddot gua = ga/omegaa \\ ddot gua = ga/omegaa \\ ddot gvc = (1/(12*omegac))*(-12*gcrL+(rL-rR)*(6*wone+9*rL^2*wthree+6*rL*rR*wthree+3*rR^2*wthree+8*rL*wtwoe+4*rR*wtwoe)) \\ ddot guc = (1/(12*omegac))*(12*gcrR+(rL-rR)*(6*wone+3*rL^2*wthree+6*rL*rR*wthree+9*rR^2*wthree+4*rL*wtwoe+8*rR*wtwoe)) \\ ddot guc = (1/(12*omegac))*(12*gcrR+(rL-rR)*(6*wone+3*rL^2*wthree+6*rL*rR*wthree+9*rR^2*wthree+4*rL*wtwoe+8*rR*wtwoe)) \\ ddot gvb = -(gb/omegab) \\ ddot gvb = -(gb/omegab)
```

1.2 Second derivatives of q (Eq. 22) with respect to the kinetic variables

1.2.1 First derivative with respect to rLdot and second derivative with respect to rLdot, rRdot, ua, vc, uc, vb total 6 terms

 $\begin{aligned} &d2qqrLdot2 = (rg*tk*(xL-xR)^3*(12*dB*rL+6*dB*rL^2-20*dB*rL^3+9*dA*rL^4-9*dB*rL^4-12*dB*rR-48*dB*rL*rR+48*dB*rL^2*rR-56*dA*rL^3*rR+56*dB*rL^3*rR+42*dB*rR^2+108*dA*rL^2*rR^2-108*dB*rL^2*rR^2-28*dB*rR^3-72*dA*rL*rR^3+72*dB*rL*rR^3+11*dA*rR^4-11*dB*rR^4+12*dB*(-1+rL)^2*(1+rL-2*rR)^2*Log[(-1+rL)*(xL-xR)]-12*dB*(-1+rL)^2*(1+rL-2*rR)^2*Log[(-1+rL)*(xL-xR)]-12*dA*rL^4*Log[rL*(-xL+xR)]+48*dA*rL^3*rR*Log[rL*(-xL+xR)]+48*dA*rL^3*rR*Log[rR*(-xL+xR)]+48*dA*rL^3*rR*Log[rR*(-xL+xR)]+48*dA*rL^3*rR*Log[rR*(-xL+xR)]+48*dA*rL^3*rR*Log[rR*(-xL+xR)]+48*dA*rL^3*rR*Log[rR*(-xL+xR)]+48*dA*rL^2*rR^2*Log[rR*(-xL+xR)]+48*dA*rL^3*rR*Log[rR*(-xL+xR)]+48*dA*rL*(-xL+xR)+48*dA*rL*(-xL+xR)+48*dA*rL*(-xL+xR)+48*dA*rL*(-xL+xR)+48*dA$

 $\begin{aligned} &d2qqrLdotrRdot = (rg*tk*(xL-xR)^3*(-12*dB*rL+18*dB*rL^2+8*dB*rL^3+19*dA*rL^4-19*dB*rL^4+12*dB*rR-60*dB*rL^2*rR-68*dA*rL^3*rR+68*dB*rL^3*rR-18*dB*rR^2+60*dB*rL*rR^2+72*dA*rL^2*rR^2-72*dB*rL^2*rR^2-8*dB*rR^3-28*dA*rL*rR^3+28*dB*rL*rR^3+5*dA*rR^4-5*dB*rR^4+12*dB*(-1+rL)^3*(1+rL-2*rR)*Log[(-1+rL)*(xL-xR)]-12*dB*(-1+rL)^3*(1+rL-2*rR)*Log[(-1+rL)*(xL-xR)]-12*dA*rL^4*Log[rL*(-xL+xR)]+24*dA*rL^3*rR*Log[rL*(-xL+xR)]+12*dA*rL^4*Log[rR*(-xL+xR)]-24*dA*rL^3*rR*Log[rR*(-xL+xR)]))/(24*dA*dB*omegac*(rL-rR)^5) \end{aligned}$

 $d2qqrLdotua = (rq*tk*(xL-xR)^2*(-2*rL-rL^2+2*rR+4*rL*rR-3*rR+4*rL*rR$ $rR^2 + 2*(-1+rL)*(1+rL-2*rR)*Log[(-1+rL)*(xL-xR)] - 2*(-1+rL)*$ $(1+rL-2*rR)*Log[(-1+rR)*(xL-xR)]))/(2*dA*omegaa*(rL-rR)^3)$ $d2qqrLdotvc = (rg*tk*(xL-xR)^2*(-12*dB*rL + 18*dB*rL^2 + 8*dB*rL^3 + 18*dB*rL^3 +$ $3*dA*rL^4 - 3*dB*rL^4 + 12*dB*rR - 60*dB*rL^2*rR - 4*dA*rL^3*rR + 4*dB*rL^4 + 12*dB*rL^4 + 12*$ $8*dB*rR^3 + 36*dA*rL*rR^3 - 36*dB*rL*rR^3 - 11*dA*rR^4 + 11*dB*rR^4 + 12*dB*rR^4 + 12*dB*rR^4 + 12*dB*rR^4 + 14*dB*rR^4 + 14*dB*rR^4$ $dB*(-1+rL)^3*(1+rL-2*rR)*Log[(-1+rL)*(xL-xR)]-12*dB*(-1+rL)^3*$ $(1+rL-2*rR)*Log[(-1+rR)*(xL-xR)]-12*dA*rL^4*Log[rL*(-xL+xR)]+$ $24*dA*rL^{3}*rR*Log[rL*(-xL+xR)]+12*dA*rL^{4}*Log[rR*(-xL+xR)] 24*dA*rL^3*rR*Log[rR*(-xL+xR)]))/(24*dA*dB*omegac*(rL-rR)^4)$ $d2qqrLdotuc = (rg*tk*(xL-xR)^2*(12*dB*rL-18*dB*rL^2-8*dB*rL^3-19*dB*rL^3-18*dB*rL^3-18*dB*rL^3-18*dB*rL^3-19*dB*rL^3-18*dB*rL^3-18*dB*rL^3-18*dB*rL^3-18*dB*rL^3-19*dB*rL^3-18$ $rL^3*rR + 18*dB*rR^2 - 60*dB*rL*rR^2 - 72*dA*rL^2*rR^2 + 72*dB*rL^2*rR^2 + 72*dB*rL^2 + 72*dB*rL^2$ $8*dB*rR^3 + 28*dA*rL*rR^3 - 28*dB*rL*rR^3 - 5*dA*rR^4 + 5*dB*rR^4 - 12*dB*rR^4 - 12*dB*rR^4$ $dB*(-1+rL)^3*(1+rL-2*rR)*Log[(-1+rL)*(xL-xR)]+12*dB*(-1+rL)^3*$ $(1+rL-2*rR)*Log[(-1+rR)*(xL-xR)]+12*dA*rL^4*Log[rL*(-xL+xR)]-12*dA*rL^4*Log[rL*(-xL+xR)]$ $24*dA*rL^{3}*rR*Log[rL*(-xL+xR)]-12*dA*rL^{4}*Log[rR*(-xL+xR)]+$ $24*dA*rL^{3}*rR*Log[rR*(-xL+xR)]))/(24*dA*dB*omegac*(rL-rR)^{4})$

1.2.2 First derivative with respect to rRdot and second derivative with respect to rRdot, ua, vc, uc, vb total 5 terms

```
d2qqrRdot2 = (rg*tk*(xL-xR)^3*(12*dB*rL-42*dB*rL^2+52*dB*rL^3+25*dA*rL^4-25*dB*rL^4-12*dB*rR+48*dB*rL*rR-72*dB*rL^2*rR-48*dA*rL^3*rR+48*dB*rL^3*rR-6*dB*rR^2+24*dB*rL*rR^2+36*dA*rL^2*rR^2-36*dB*rL^2*rR^2-4*dB*rR^3-16*dA*rL*rR^3+16*dB*rL*rR^3+3*dA*rR^4-3*dB*rR^4+12*dB*(-1+rL)^4*Log[(-1+rL)*(xL-xR)]-12*dB*(-1+rL)^4*Log[(-1+rR)*(xL-xR)]-12*dA*rL^4*Log[rL*(-xL+xR)]+12*dA*rL^4*Log[rR*(-xL+xR)]))/(24*dA*dB*omegac*(rL-rR)^5)
```

 $\begin{array}{l} d2qqrRdotua = (rg*tk*(xL-xR)^2*(2*rL-3*rL^2-2*rR+4*rL*rR-rR^2+2*(-1+rL)^2*Log[(-1+rL)*(xL-xR)]-2*(-1+rL)^2*Log[(-1+rR)*(xL-xR)]))/(2*dA*omegaa*(rL-rR)^3) \end{array}$

 $\begin{aligned} d2qqrRdotvc &= (rg*tk*(xL-xR)^2*(12*dB*rL-42*dB*rL^2+52*dB*rL^3+17*dA*rL^4-17*dB*rL^4-12*dB*rR+48*dB*rL*rR-72*dB*rL^2*rR-16*dA*rL^3*rR+16*dB*rL^3*rR-6*dB*rR^2+24*dB*rL*rR^2-12*dA*rL^2*rR^2+12*dB*rL^2*rR^2-4*dB*rL^3+16*dA*rL*rR^3-16*dB*rL*rR^3-5*dA*rR^4+5*dB*rR^4+12*dB*(-1+rL)^4*Log[(-1+rL)*(xL-xR)]-12*dB*(-1+rL)^4*Log[(-1+rR)*(xL-xR)]-12*dA*rL^4*Log[rL*(-xL+xR)]+12*dA*rL^4*Log[rR*(-xL+xR)]))/(24*dA*dB*omegac*(rL-rR)^4) \end{aligned}$

 $d2qqrRdotuc = (rg*tk*(xL-xR)^2*(-12*dB*rL+42*dB*rL^2-52*dB*rL^2+12*dB*rL^4+25*dB*rL^4+12*dB*rR-48*dB*rL*rR+72*dB*rL^2*rR+48*dA*rL^3*rR-48*dB*rL^3*rR+6*dB*rR^2-24*dB*rL*rR^2-36*dA*rL^2*rR^2+36*dB*rL^2*rR^2+4*dB*rR^3+16*dA*rL*rR^3-16*dB*rL*rR^3-3*dA*rR^4+3*dB*rR^4-12*dB*(-1+rL)^4*Log[(-1+rL)*(xL-xR)]+12*dB*(-1+rL)^4*Log[(-1+rL)*(xL-xR)]+12*dA*rL^4*Log[rR*(-xL+xR)]))/(24*dA*dB*omegac*(rL-rR)^4)$

d2qqrRdotvb=0

1.2.3 First derivative with respect to ua and second derivative with respect to ua, vc, uc, vb total 4 terms

$$\begin{split} d2qqua2 &= (dA*fvua^2*omegaa^2*(rL-rR)*(4*mac+uac) + 4*mac*omegac*rg*tk*uac*(xL-xR)*Log[(-1+rL)*(xL-xR)] + 4*mac*omegac*rg*tk*uac*(-xL+xR)*Log[(-1+rR)*(xL-xR)])/(2*dA*mac*omegaa^2*(rL-rR)*uac) \end{split}$$

 $\begin{aligned} d2qquavc &= (1/2)*((fvua*fvvc)/mac - (4*fvua*fvvc)/uac + (rg*tk*(xL-xR)*(2*rL+rL^2-2*rR-4*rL*rR+3*rR^2+2*(-1+rL)^2*Log[(-1+rL)*(xL-xR)] - 2*(-1+rL)^2*Log[(-1+rR)*(xL-xR)]))/(dA*omegaa*(rL-rR)^2)) \end{aligned}$

```
\begin{split} d2qquauc &= -((rg*tk*(xL-xR)*(2*rL-3*rL^2-2*rR+4*rL*rR-rR^2+2*(-1+rL)^2*Log[(-1+rL)*(xL-xR)]-2*(-1+rL)^2*Log[(-1+rR)*(xL-xR)]))/(2*dA*omegaa*(rL-rR)^2)) \\ d2qquavb &= 0 \end{split}
```

1.2.4 First derivative with respect to vc and second derivative with respect to vc, uc, vb total 3 terms

 $\begin{aligned} &d2qqvc2 = fvvc^2/(2*mac) + (2*fvvc^2)/uac + (rg*tk*(xL - xR)*(12*dB*rL - 42*dB*rL^2 + 4*dB*rL^3 - 15*dA*rL^4 + 15*dB*rL^4 - 12*dB*rR + 48*dB*rL*rR + 72*dB*rL^2*rR + 64*dA*rL^3*rR - 64*dB*rL^3*rR - 6*dB*rR^2 - 120*dB*rL*rR^2 - 60*dA*rL^2*rR^2 + 60*dB*rL^2*rR^2 + 44*dB*rR^3 + 11*dA*rR^4 - 11*dB*rR^4 + 12*dB*(-1+rL)^4*Log[(-1+rL)*(xL - xR)] - 12*dB*(-1+rL)^4*Log[(-1+rR)*(xL - xR)] - 12*dA*rL^4*Log[rL*(-xL + xR)] + 12*dA*rL^4*Log[rR*(-xL + xR)]))/(24*dA*dB*omegac*(rL - rR)^3) \end{aligned}$

 $d2qqvcuc = (rg*tk*(xL-xR)*(-12*dB*rL+42*dB*rL^2-52*dB*rL^3-17*dA*rL^4+17*dB*rL^4+12*dB*rR-48*dB*rL*rR+72*dB*rL^2*rR+16*dA*rL^3*rR-16*dB*rL^3*rR+6*dB*rR^2-24*dB*rL*rR^2+12*dA*rL^2*rR^2-12*dB*rL^2*rR^2+4*dB*rR^3-16*dA*rL*rR^3+16*dB*rL*rR^3+5*dA*rR^4-5*dB*rR^4-12*dB*(-1+rL)^4*Log[(-1+rL)*(xL-xR)]+12*dB*(-1+rL)^4*Log[(-1+rL)*(xL-xR)]+12*dA*rL^4*Log[rR*(-xL+xR)]))/(24*dA*dB*omegac*(rL-rR)^3)$

d2qqvcvb = 0

1.2.5 First derivative with respect to uc and second derivative with respect to uc, vb total 2 terms

```
\begin{aligned} &d2qquc2 = fvuc^2/(2*mcb) + (2*fvuc^2)/ucb + (rg*tk*(xL - xR)*(12*dB*rL - 42*dB*rL^2 + 52*dB*rL^3 + 25*dA*rL^4 - 25*dB*rL^4 - 12*dB*rR + 48*dB*rL*rR - 72*dB*rL^2*rR - 48*dA*rL^3*rR + 48*dB*rL^3*rR - 6*dB*rL^2 + 24*dB*rL + rR^2 + 36*dA*rL^2*rR^2 - 36*dB*rL^2*rR^2 - 4*dB*rR^3 - 16*dA*rL*rR^3 + 16*dB*rL*rR^3 + 3*dA*rR^4 - 3*dB*rR^4 + 12*dB*(-1+rL)^4*Log[(-1+rL)*(xL - xR)] - 12*dB*(-1+rL)^4*Log[(-1+rR)*(xL - xR)] - 12*dA*rL^4*Log[rL*(-xL + xR)] + 12*dA*rL^4*Log[rR*(-xL + xR)])/(24*dA*dB*omegac*(rL - rR)^3) \\ &d2qqucvb = (1/2)*fvuc*fvvb*(1/mcb - 4/ucb) \end{aligned}
```

1.2.6 second derivative with respect to vc - 1 term

$$d2qqvb2 = (fvvb^2 * (4 * mcb + ucb))/(2 * mcb * ucb)$$

2 Layer growth in Al_2O_3 -MgO system: experimental

2.1 Layer growth experiments

Rectangular prisms (3 by 3 by 5 mm) of corundum and periclase single crystals with known crystallographic orientations were assembled in a stack, whereby polished faces were used to make contact. The assembly was put into a deadload uniaxial creep apparatus at Helmholtz Zentrum Potsdam, Deutsches GeoForschungsZentrum using a procedure described in detail by Götze et al. (?). A uniaxial load of 0.26 kN corresponding to a normal stress of 29 MPa when calculated for a 9 mm² cross section was applied to ensure good mechanical contact. Annealing temperature was 1350°C, heating and cooling rates were 5°C/min. Durations of the experiments were 5 to 160 h. After experiment the samples were embedded in epoxy and cut perpendicular to the reaction interface for preparation of polished thin sections.

2.2 Microstructure and texture analysis

Polished cross sections of the reaction rims were investigated using a FEI Quanta 3D Field Emission Gun (FEG) instrument at the Laboratory for electron microscopy and focused ion beam applications of the Faculty of Geosciences, Geography and Astronomy, University of Vienna, Austria. The FEG-SEM is equipped with an EDAX Digiview IV EBSD camera and an Apollo XV silicon drift detector for Energy Dispersive X-ray (EDX) spectrometry. For a detailed description of the instrumental settings used see (?).

2.3 Composition analysis

The chemical composition of spinel was analyzed at Helmholtz Zentrum Potsdam, Deutsches GeoForschungsZentrum using a Jeol JXA-8500F field-emission gun electron-probe micro analyzer. Analytical conditions were 50 nm focus spot, 10 nA beam current, 6 kV accelerating voltage and 40 seconds counting time on the peak and 20 seconds counting time on the background on either side of the peak. A step size of 500 nm was used for analyses along profiles across the spinel layers. A liquid nitrogen trap was used to reduce carbon contamination. Both, aluminium and magnesium were analyzed on TAP crystals. Calibration was done on pure corundum and periclase crystals, respectively, from the sample. The CITZAF routine was applied for matrix correction.

2.4 Microstructure, texture and composition of spinel

Where the contact plane is perfectly smooth, the newly grown spinel forms layers of relatively constant thickness (Fig. 1). Substantial lateral variations in layer thickness do, however, occur, where the reactant periclase and/or corundum are deformed due to the applied load (?). In most instances, the spinel

layer consists of two microstructurally and texturally distinct domains (???). About one fifth of the layer thickness on the side of periclase is made up by spinel with columnar grains, which show fully topotactic relations to periclase so that $(100)_{\rm per} \parallel (100)_{\rm sp}$ and $(111)_{\rm per} \parallel (111)_{\rm sp}$. The columnar microstructure of the spinel is due to subtle rotations of the spinel individuals (less than about 2° misorientation) with respect to one another. The periclase-spinel interface is probably semi-coherent with one mismatch dislocation in about 25 lattice planes to compensate for the about 4% lattice mismatch at the interface (?). About four fifth of the layer thickness on the side of corundum show topotactic relations to corundum so that $(0001)_{cor} \parallel (111)_{sp}$ and $[1\bar{1}00]_{cor} \parallel [0\bar{1}1]_{sp}$ or $[1\bar{1}00]_{cor} \parallel [01\bar{1}]_{sp}$. Such topotaxy was reported earlier (????). It ensures that close-packed oxygen planes and close-packed directions in these planes are inherited from corundum by the newly formed spinel. Spinel grains adhering to the two different in-plane orientations are related by the spinel twin law (60°) rotation about the $[111]_{sp}$ -axis). As shown by the use of inert markers (?) the microstructural and textural discontinuity within the spinel layer reflects the original contact between reactant periclase and corundum.

It is interesting to note that sub-micrometer sized pores typically occur at the periclase-spinel contacts. Whereas the reaction interface is smooth on the scale of the dimension of the entire reaction rim, it is rugged on the micrometer scale due to the pinning effect of the pores (Fig. 1c). No such pores and roughness occur at the spinel-corundum interface. This is ascribed to the semi-coherent nature of the periclase-spinel interface. Such an interface is likely rather inefficient in generating/annihilating vacancies. If Schottky defects are introduced by removal of MgO from this interface, there is little chance for those to be annihilated at the interface. If the interface region becomes successively more oversaturated with vacancies, this may eventually lead to the nucleation and growth of pores. Such pores will, in turn, reduce the overall mobility of the reaction interface due to their pinning effect.

3 Layer growth in Al₂O₃-MgO system: thermodynamics

3.1 Equilibrium phase relations

Phase diagrams constructed using Thermocalc Version S based on a re-assessment of the thermodynamic data by (?) are shown in figure 2. We are interested in the equilibrium solubility range of spinel, which is indicated by the black horizontal bar in figure 2.

3.2 Approximation of Gibbs energy for spinel

For applying the thermodynamic model the Gibbs energy of spinel must be approximated by a polynomial. Phase equilibrium constraints are derived from periclase-spinel and corundum-spinel equilibria based on thermodynamic data

by (?). Four constraints are obtained:

- (1) The Gibbs energy and the composition of spinel in equilibrium with periclase are known from Thermocalc calculations.
- (2) The slope $\frac{\partial g}{\partial r_{Al_2O_3}}$ at this composition is known from Thermocalc calculations
- (3) The Gibbs energy and the composition of spinel in equilibrium with corundum are known from Thermocalc calculations.
- (4) The slope $\frac{\partial g}{\partial r_{Al_2O_3}}$ at this composition is known from Thermocalc calculations

To satisfy all four constraints, g(r) must be approximated as a third order polynomial. It must be noted that a more rigorous formulation would involve the term $R_gT(r\ln r + (1-r)\ln(1-r))$ with R_g being the gas constant and T the absolute temperature, which accounts for configurational entropy. In the problem at hand the solubility range of spinel is small with $(r_R - r_L) << 1$. In this case the configurational entropy term is nearly a constant, and is accounted for by W_0 in the simplified Gibbs energy model. The polynomial approximation is compared to g(r) as directly obtained from Thermocalc and to a model including the configurational entropy term in figure 3. It is important to note that this approximation can only be used reliably between the two equilibrium compositions of spinel. Extrapolation beyond this composition range needs to be done with caution, as an inflection point may occur, which would produce erroneous convex hull of the Gibbs energy composition space. In the application at hand the approximation of g(r) is only used in the composition range between the two equilibrium compositions.

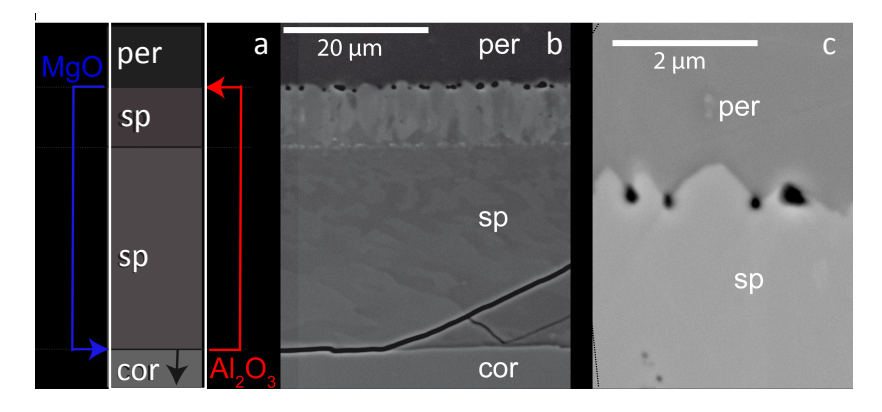


Figure 1: a: schematic sketch of rim growth setting; b: BSE image of spinel (sp) layer forming at the contact between periclase (per) and corundum (cor) single crystals; different grey shades within spinel reflect different lattice orientations; microstructural discontinuity within spinel traces the original periclase-corundum contact (Kirkendall plane); c: detail of the periclase-spinel interface with pores dragged along with the propagating reaction interface; note that the spinel-corundum interface is devoid of pores.

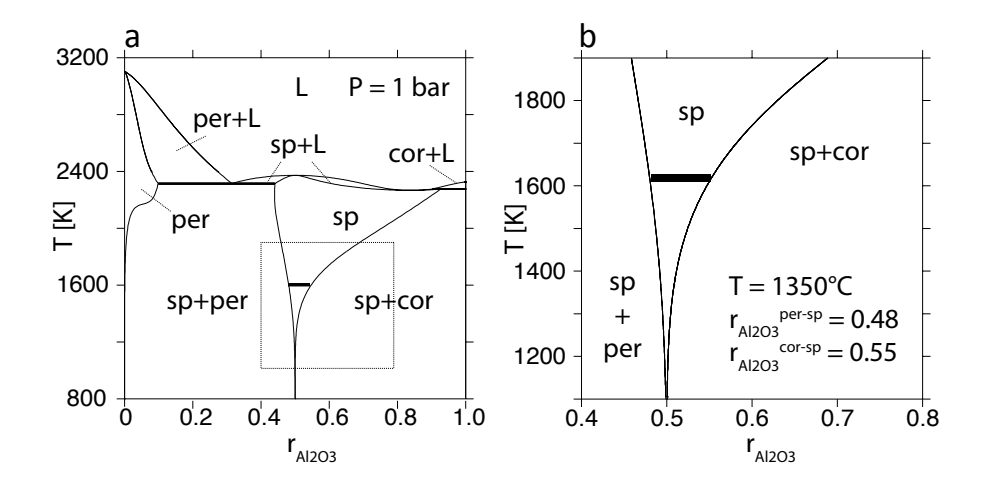


Figure 2: a: phase diagram for the system MgO-Al₂O₃ for atmospheric pressure constructed using Thermocalc Version S, based on thermodynamic data by Zienert and Fabrichnaya (?); reactangular box shows composition - temperature range of the close up view in b; b: detail of the phase relations of spinel in the temperature - composition range of interest; horizontal black bar shows the range of stable spinel compositions at the conditions of the experiments.

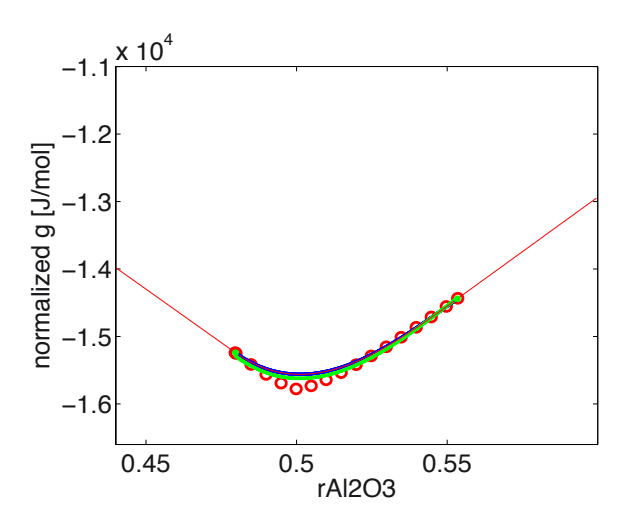


Figure 3: open red circles represent g-values of spinel as obtained form Thermocalc, green curve shows the approximation by a third order polynomial augmented with the configurational energy term; blue curve shows the approximation by a third order polynomial accounting for the nearly constant configurational energy term in W_0 ; green circles indicate the equilibrium compositions in contact with periclase (left) and with corundum (right).